Analysis of the impact of floater interactions on the power extraction of a dense WEC array with adaptable nonlinear PTO

A. Bechlenberg, Y. Wei, B. Jayawardhana, and A. I. Vakis

Abstract—**This research focuses on studying the interactions between a closely spaced wave energy converter (WEC) array with an adaptable hydraulic power take-off (PTO) system. The boundary element method is used to extract the hydrodynamic and hydrostatic coefficients, while the power extraction and hydrodynamic behaviour of the array are simulated in irregular waves with a mixed frequency-time-domain (MFT) model to include the nonlinear PTO forces of each array element. The interactions between floaters are assessed and the influence of adaptability on the behaviour of the total array and its elements in comparison to single floater performance (i.e., the q factor) is analysed. The differences in performance of the WEC array are assessed with three levels of adaptability: no adaptability, adaptability per sea state and adaptability per incoming wave.**

Index Terms—**interaction effects, dense WEC array, power absorption, hydraulic PTO, adaptability**

I. Introduction

WAVE energy has the potential to increase the share of renewables in the energy mix to meet the increasing demand. While a number of single wave energy converters have reached high technology readiness levels, their commercialisation has faced challenges due to the high levelized cost of electricity (LCOE). Correspondingly, recent research and development has focused on creating arrays of WECs in co-location with or embedded within hybrid offshore renewable energy systems to increase the power absorption per ocean area and decrease the levelised cost of electricity by sharing infrastructure and operation and maintenance costs [1]. Furthermore, WEC arrays have been shown to broaden the bandwidth of power extraction and to increase the total power extraction by constructive interaction effects between array elements [2]–[4].

Past research has focused on the optimisation of the geometry and arrangement of WEC arrays, as well as on the power take-off (PTO) systems used [2], [5]–[7]. Due to computational complexity and costs, once the single WEC has been fully designed and optimised, less emphasis is placed on the layout of an array (or farm) and the focus is shifted to the behaviour of single WECs [8]. Especially in closely spaced WEC arrays, it is crucial to study the interactions between the elements thoroughly. Initially, it was found by simulating an array with a Boundary Element Method (BEM) that more than ten devices (of dimensions between 10-20m) and short separating distances showed negative effects that would influence the power output significantly and, therefore, such designs should be avoided [9]. By comparing a numerical model and experimental testing of a WEC array, it was shown that the numerical model overestimates the interactions, but averaging out this effect throughout the simulation leads only to small differences; furthermore, in both methods, the same array configuration showed the maximum output and the performance of the elements in the array decreased in the direction of the incoming wave, while elements at the borders of the configuration showed weaker interaction effects [10]. In other research, it was shown that triangular array configurations performed best for multidirectional waves and increasing the number of elements of the array could lead to an increase in positive interactions [4].

Different subsystems of the WEC such as the PTO system and its control strategies can also influence the behaviour and interactions [11]. Previous research focusing on comparing a single WEC with an array by applying a linear BEM and a nonlinear computational fluid dynamics (CFD) model showed that, with a linear PTO system acting on the pitch motion, the linear BEM overestimated the power extraction but showed satisfactory consistency in the absence of a PTO force [12]. The tuning of each element in an array and the total number of elements were proven to significantly influence the total power output and the selection of the optimal tuning, especially for arrays with significant interaction effects [13], [14]. Other research focusing on arrays with a direct-linear PTO suggests that, by optimising the single floater, an array also performs optimally [15]. In specific cases, the PTO is designed as a hydraulic system; nonlinear forces are then introduced which significantly affect the mass and inertia and, thus, the motion of the floater of the WEC. A review of existing models that include nonlinear forces for the simulation of WECs highlights the complexity and importance of selecting the correct

A. Bechlenberg is with the CMME group at ENTEG, University of Groningen, the Netherlands (e-mail: a.bechelenberg@rug.nl).

Y. Wei is at the Eastern Institute for Advanced Study, Yongriver Institute of Technology, Ningbo, Zhejiang, China, 315201 (e-mail: yanji.wei@eias.ac.cn).

B. Jayawardhana is with the DTPA group at ENTEG, University of Groningen, the Netherlands (e-mail: b.jayawardhana@rug.nl).

A. I. Vakis is with the CMME group at ENTEG, University of Groningen, the Netherlands (e-mail: a.vakis@rug.nl).

Digital Object Identifier:
https://doi.org/10.36688/ewtec-2023-310

forces that must be included in simulations [8].

A clear definition and assessment of all factors affecting the development of WECs makes it clear that the design process for wave energy projects is very complex [16] and that, depending on the location, stakeholders and application, the devices most suitable for deployment vary considerably [17]. Currently, a lack of overarching procedures that can be applied by all developers leads to very different and often iterative paths of development; it is necessary to include crucial decision factors from the beginning of the development and design process [18]. In fact, the choice of assumptions made in the optimisation of a WEC design might finally lead to a suboptimal solution.

This research studies the interactions between elements of a dense array in irregular waves including the effects of a central, fixed pillar, as well as nonlinear PTO forces and the adaptability of the PTO system. The aim is to understand which parameters effect the WEC array performance and adapt the design of the WEC array accordingly. The applied model increases the complexity of the simulations in terms of the behaviour of the array elements by including the nonlinear PTO forces so as to provide insight into more realistic effects while also considering the computational efforts necessary for these simulations. The results can be used to choose the adaptability range and dimensions of a nonlinear piston-pump PTO system for a location-dependent WEC array.

II. Methodology

A. Equation of motions

Based on linear potential flow theory, the motion equation of each element of the WEC array is governed by the following force balance:

$$\boldsymbol{M}_b\ddot{\boldsymbol{X}}_b = \boldsymbol{F}_{\text{ex}} + \boldsymbol{F}_r + \boldsymbol{F}_{hs} + \boldsymbol{F}_c, \tag{1}$$

with $\boldsymbol{M}_b$ being the mass of the buoy, $\ddot{\boldsymbol{X}}_b$ the acceleration of the buoy and $\boldsymbol{F}_{\text{ex}}$, $\boldsymbol{F}_r$, $\boldsymbol{F}_{hs}$, and $\boldsymbol{F}_c$ being the excitation, radiation, hydrostatic restoring and cable forces, respectively. The variable $\boldsymbol{F}_c$ characterises the force of the PTO system onto the buoy through the connecting cable. The internal equation of motion of the hydraulic PTO system is given by

$$m_p\frac{\ddot{X}_b}{\alpha} = -F_p - \alpha F_c, \tag{2}$$

where m_p is the mass of the piston, F_p is the pumping force and α is the transmission ratio which enables the PTO adaptability. The pumping force is characterised by the hydraulic head, the inertia effect and kinetic energy losses in the system. The hydraulic PTO considered herein is only activated in the upwards motion and its position is reset in the downstroke; this nonlinear behaviour is defined in relation to the velocity of the piston as follows:

$$F_p = \begin{cases} \left[\rho g\left(D-h_r\right) + \rho l_p\ddot{z}_p + \rho\dot{z}_p^2\right]A_c & \text{if } \dot{z}_p > 0 \\ 0 & \text{otherwise,} \end{cases} \tag{3}$$

where ρ is the density of the working fluid inside the PTO system, D is the water depth at the deployment location, h_r is the water level in the internal (rigid) reservoir, l_p is the length of the PTO piping between the two reservoirs, A_c is the area of the piston and z_p is the displacement of the piston. More information on the PTO design can be found in [19].

To analyse the entire system including the influences of the PTO and the adaptability on the floaters, (1) and (2) are combined to arrive at the following equation of motion

$$\left(M_b + \frac{m_p}{\alpha^2}\right)\ddot{X}_b = F_{\text{ex}} + F_r + F_{hs} - \frac{F_p}{\alpha}. \tag{4}$$

B. Mixed Frequency-Domain Time-Domain Model

The numerical model utilised herein to solve the equations of motion of the WEC array is a mixed frequency-domain/time-domain (MFT) model introduced and validated in previous research [20]. The nonlinear motion of the array is solved iteratively, with a harmonic balance method (HBM) [21], [22] applied in the frequency domain while computing the nonlinear PTO force in the time domain. By splitting the total simulation into time windows, the motion equation is described with a number of harmonic components and the nonlinear term is solved in the time-domain for each time window with the Lagrange multipliers method. This model is in good agreement with time domain simulations but does show difficulties in occasions in which the excitation force does not overcome the pumping force, as this behaviour requires that higher harmonics be included, which would significantly increase the computational time [8], [20].

The MFT model makes it possible to simulate a large number of cases in irregular waves by using sea states described through peak period T_p and significant wave height H_s and a range of α values to study the effect of PTO adaptability on a dense WEC array. Considering that X_b, F_{ex}, F_r, F_{hs} and F_p are approximated as a truncated Fourier series, it is possible to describe the n-th harmonic motion equation of the i-th element based on (4) as

$$\left[-n^2\omega^2\left(M_{b,n}^{(i)} + \frac{m_p^{(i)}}{\alpha^2} + A_{r,n}^{(i,i)}\right) + in\omega B_{r,n}^{(i,i)} + K_{hs,n}^{(i)}\right]\hat{X}_{b,n}^{(i)} + \sum_{j=1,j\neq i}^{N_b}\left(-n^2\omega^2 A_{r,n}^{(i,j)} + in\omega B_{r,n}^{(i,j)}\right)\hat{X}_{b,n}^{(j)} + \frac{\hat{F}_{p,n}^{(i)}}{\alpha} = \hat{F}_{ex,n}^{(i)}, \tag{5}$$

with $A_{r,n}$, $B_{r,n}$, $K_{hs,n}$ being the added mass, radiation damping and hydrostatic coefficients and N_b being the total number of floaters. The interactions between elements of the array are included in the first order wave loads ($A_{r,n}$, $B_{r,n}$ and $\hat{F}_{ex,n}$) based on the results of the open source BEM model NEMOH; these variables describe the motion of each floater but also cross-coupling effects, although they are not modelled through the nonlinear approach. The time window length is defined as twice the peak period and an overlap between time windows ensures that the memory effect from the previous wave is considered.

The motion equation can be summarised as

$$Z_r \tilde{X}_b + \frac{\tilde{F}_p}{\alpha} = \tilde{F}_{\text{ex}}, \tag{6}$$

with Z_r being the condensed stiffness matrix including all interactions described in (5), $\tilde{X}_b$ being the vector of displacement of all floaters including the Fourier coefficients of real and imaginary parts of the frequency domain displacement, $\tilde{F}_p$ being the pumping force, and $\tilde{F}_{\text{ex}}$ being the excitation force in the frequency domain. This is utilised to generate the time domain equations' discrete (inverse) Fourier transform matrices (T and T_{inv}) to switch between the two domains:

$$f(\tilde{X}_b) = \bar{F}_{\text{ex}} - T Z_r \tilde{X}_b + \frac{\bar{F}_p}{\alpha}, \tag{7}$$

in which the floaters' displacement is solved with the time domain forces of excitation $\bar{F}_{\text{ex}}$ and pumping $\bar{F}_p$.

The PTOs act on the heave motion, thus, the simulations only consider this degree of freedom (DoF) and its influence on the other elements' heave motion; due to the design of the dense WEC array, the other DoF are assumed to be minimised as much as possible (through physical constraints) not only to increase the power extraction but also to avoid collisions.

The MFT model is used to simulate the power absorption and element behaviour in a range of sea states using the above mentioned parameters H_s and T_p which are set to the ranges presented in Table I; a power matrix can summarise the performance of the studied WEC design by showing the total power absorbed in each sea state.

C. Comparison Metrics

To compare the WEC array's performance with a single floater and highlight the effect of interactions, the commonly used q factor and interaction factor are selected [7], [10], [23]. The interaction factor,

$$q_n = \frac{P_n}{P_{\text{SF}}}, \tag{8}$$

is a ratio between the power generated by the n-th floater of the array compared to a stand-alone single floater (SF). The q factor is based on the same principle but compares the total power generated by the array with the possible power generated by the same amount of stand-alone WECs without interaction effects:

$$q = \frac{P_{\text{Array}}}{N_b P_{\text{SF}}}. \tag{9}$$

When these factors are > 1, interaction effects of the array are of constructive nature, while, if they are < 1, the single floater placed at sufficiently large distance so as not to interact with its neighbouring WECs would generate more power – destructive effects are dominating the array's performance.

III. Case Study

To study the interactions between floaters and the effect of PTO adaptability, an 18 element array is analysed. The shape of each floater and the array configuration are depicted in Fig. 1 and the dimensions are

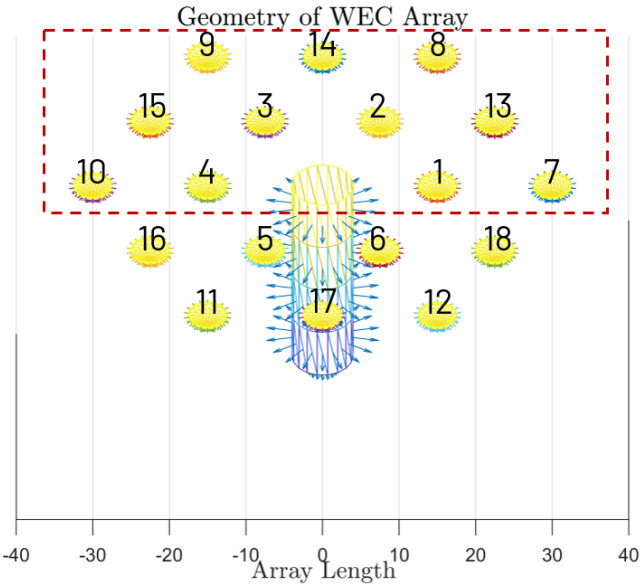

Fig. 1: Geometry and array configuration from NEMOH

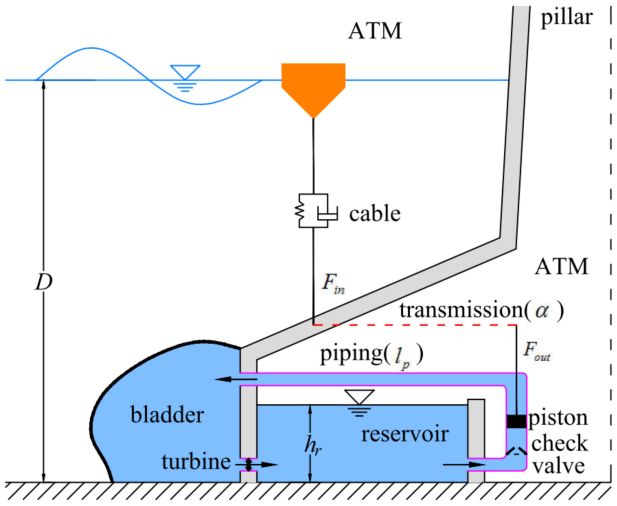

Fig. 2: Internal subsystem including the PTO system. Partially reprint from [19]

summarised in Table I. The array is considered closely spaced, with a distance between floaters of twice their diameter; thus, it is assumed that a support structure is in place that ensures that the configuration remains fixed and the floaters are free to move in heave. This could increase the deployability of the design as the costs for mooring and connecting lines could decrease and the extracted power might increase through the application of connected devices [24]. The floaters are arranged in a honeycomb formation around a fixed central pillar, which is designed to house an offshore wind turbine. The floater numbers shown in Fig. 1 are used as reference to explain the interaction effects of specific elements of the array in section IV. Due to the symmetry on the xz plane, the results will focus on the top part of the array shown in a red box in Fig. 1; in previous research, the array was also grouped into horizontal and vertical sections to highlight different behaviour of specific elements [19].

TABLE I: Parameters of the simulation and the studied system

	Description	Symbol	Quantity	Unit
WEC array	Diameter of Floater	d_b	5	m
	Draft of Floater	D_b	3	m
	Buoy Mass	m_b	15,000	kg
	Number of Floaters	N_b	18	-
	Width of Array	B	52	m
	Water Depth	D	60	m
PTO	Transmission Ratio	α	[0.1–2]	-
	Piston Mass	m_p	1,000	kg
	Working Fluid Density	ρ	1,025	$\frac{kg}{m^3}$
	Piston Radius	d_p	0.3449	m
	Piping Length	l_p	30	m
	PTO Efficiency	η_p	0.9	-
Simulation	Peak Period	T_p	[3–14]	s
	Significant Wave Height	H_s	[0.5–8]	m

Each floater is connected to a hydraulic piston-pump PTO system enclosed in the gravity based foundation on the seabed (Fig. 2). The pumping force of the PTO system depends on the depth at the deployment location, as seen in Eq. 3, as it exploits the pressure difference between the rigid internal reservoir inside the gravity based foundation (at atmospheric pressure ATM) and an external bladder reservoir (with the hydrostatic pressure based on the depth at the deployment location). Based on the analysis of the adaptability in frequency domain simulations [19], the piston-pump initial design is tuned to the most energetic sea states of the location. The location selected is far offshore in the North Sea; a thorough investigation of the potential of this location can be found in [25], [26]. The ratio between the hydrostatic force (hydraulic head) of the PTO system (as described in Eq. 3) and the mean absolute excitation force in the predefined sea states (SS), is applied to define an initial size for the piston's radius in the case of no adaptability ($\alpha = 1$),

$$\alpha = \frac{\rho g (D - h_r) A_p}{2|F_{ex,SS}|} = 1. \tag{10}$$

As the hydraulic head is approximated to be half of the total pumping force, it is compared to half of the excitation force.

A. Adaptability Levels

Different adaptability degrees can be assessed with an exhaustive search approach on the results of the MFT model [25]. For each sea state simulation, the performance of the WEC design is compared for different values of α chosen from the transmission ratio range (Table I); decreasing the timescale at which α is selected increases the adaptability level. Adapting α for each total simulation of one sea state means that the transmission ratio is selected to be constant for the entire sea state. When adapting α per time window, the transmission ratio is selected for each time window within each sea state simulation. As mentioned above, the time window length is defined as twice the peak period of the sea state, which would mean that the WEC is tuned to each incoming wave (considering that an overlap between time windows is applied at the beginning and end of each time window). The transmission ratio is applied consistently to all floaters as, for this research, it is not yet possible to adapt α for each floater separately.

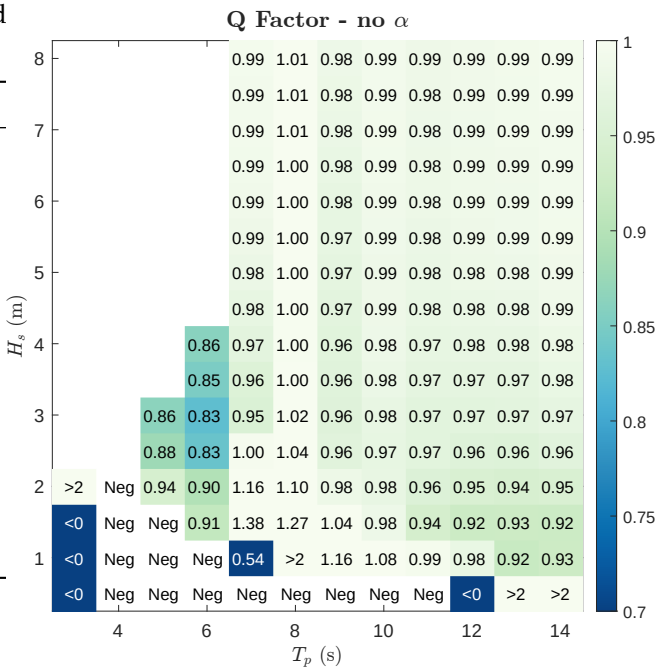

Fig. 3: The q factor of the array without inclusion of PTO adaptability ($\alpha = 1.0$)

IV. Results

A. Interaction between floaters without adaptability

Before assessing the effect of PTO adaptability (through α) on the performance and interactions of the WEC array in comparison to the performance of a single floater, the interaction effects and WEC array performance is assessed without PTO adaptability ($\alpha = 1.0$).

1) Q Factor of Array: Fig. 3 shows the q factor of the array for each sea state; in most sea states the q factor is above 0.9, while at short T_p it decreases and at low H_s the q factor shows stronger fluctuations. Some noteworthy results at low H_s and T_p are:

- Negative power absorbed by the array due to numerical errors, which were mentioned above as one of the limitations of the model, are not considered as they do not have physical significance; nevertheless, previous investigation into the causes for this behaviour point to potential sticking of the PTO system [20], [25]. These can be seen as white fields in the matrix denoted with 'Neg'.
- Negative q factor due to negative power absorption of the single floater but not of the array, marked with '< 0' in the figure.
- Q factor larger than 2, noted with '> 2' in the matrix.

The sea states in which these occur are outside the design scope of the floater and PTO system design.

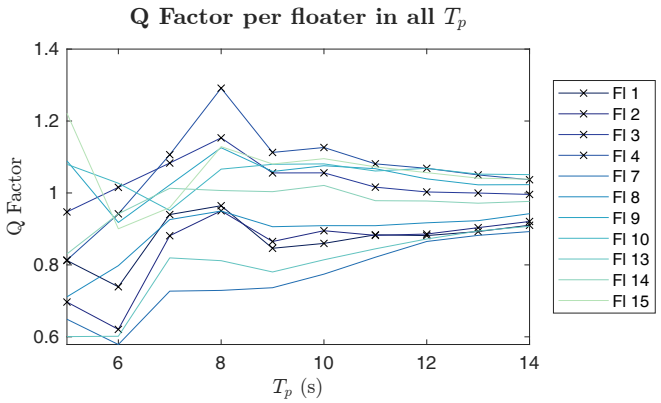

Fig. 4: The Q factors of selected floaters of the array at sea states with H_s 3m shows the different peaks of the floaters with changing T_p

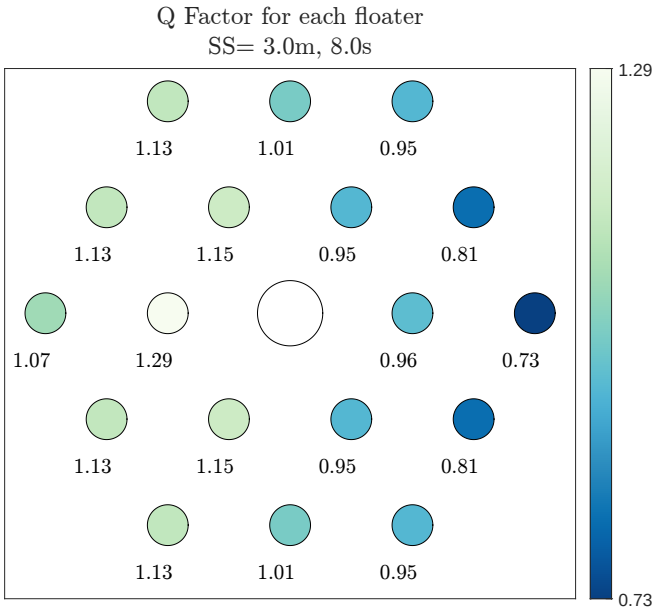

Fig. 5: The Q factors of all floaters of the array at sea state H_s 3m and T_p 8s show the positive effect of the central pillar.

Further analysis of the results will not focus on these sea states.

In the sea states in which the q factor is within the conventional range of 0 and 1, it can be observed that a dip occurs around $T_p = 6s$, while at $T_p = 8s$ and less notably at $T_p = 10s$ a trend can be seen that the array improves its performance even outperforming the single floater in specific cases.

2) Q Factor of individual elements: By analysing the q factor of each element in the array, it becomes clear that most energy is extracted by the first row of floaters and decreases in the wave direction. However, based on their position dips and peaks can be seen at different T_p which lead to a more constant q factor of the total array (as can be seen in 3). This is shown in Fig. 4; to highlight the floater in the internal circle their plots are marked.

The influence of the fixed central pillar is worth highlighting; the detailed analysis per element of the array shows that not only does the floater position in regards to the incoming wave influence their performance, but also the central pillar significantly affects the outcome.

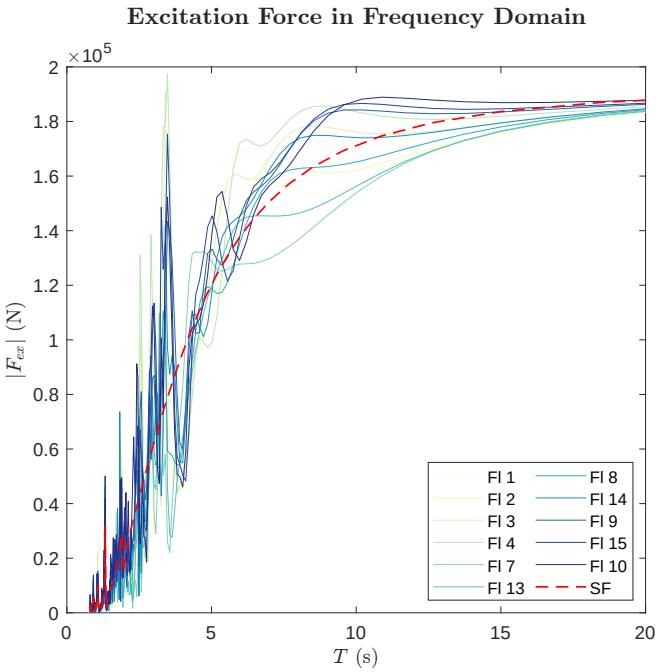

Fig. 6: Absolute excitation force in frequency domain for the single floater and half of the elements in the WEC array

In certain sea states, as can be seen in Fig.5, the floaters adjacent to the pillar outperform the floaters on the outside circle. With increasing T_p, the q factor becomes more influenced by the incoming wave and floaters at the front of the array show higher power extraction.

3) Excitation and radiation forces: In order to contextualise these results, the diffraction and radiation forces are analysed more thoroughly. The absolute excitation force ($|F_{\text{ex}}|$) is analysed in the frequency domain to understand the diffraction forces and the root mean square (RMS) of the radiation force ($F_{r,\text{RMS}}$) in each sea state is computed from the time domain results as this includes the actual displacement of all floaters as well as the influences of the heave motions of all the elements onto each other's behaviour (as mentioned in relation to (5)). Only the excitation forces of the 11 floaters highlighted in Fig. 1 are depicted in Fig. 6.

From the excitation force in the frequency domain, it is clear to see that at short periods (high frequency) irregular frequency effects, which are characteristic of BEM models, and high fluctuations can be seen in both single floater and the array dynamics. In the array, these are larger and appear for a longer span of periods (up until 4s); as the nonlinearities occur only until 2s for the single floater, it can also be argued that the effects after that period occur because of the diffraction forces between floaters. While the single floater shows a steady increase in $|F_{\text{ex}}|$, elements of the array have local (or global) maxima. Taking into consideration the differences between q factors of the individual elements (as in Fig.4), the first floaters in the wave direction show high excitation force at lower regular frequency, T, while the floaters in front of the central pillar show a higher excitation force at slightly higher T and many floaters have a higher $|F_{\text{ex}}|$ than the single floater at T 10s. In longer periods, it is visible that all floaters approximate the excitation force of the single

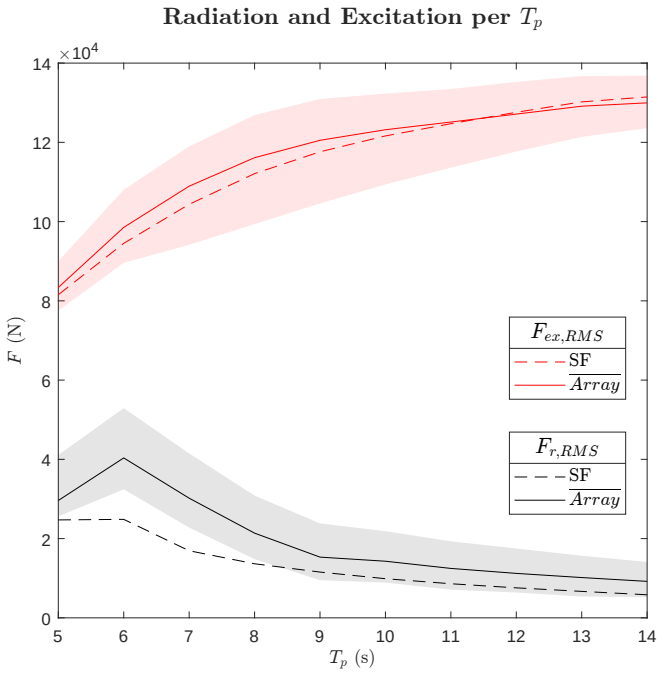

Fig. 7: Root mean square (RMS) of the excitation force and radiation force of the single floater, the mean of the array and the range of each floater in the array without inclusion of PTO adaptability ($\alpha = 1.0$) at the all sea states with $H_s = 3m$

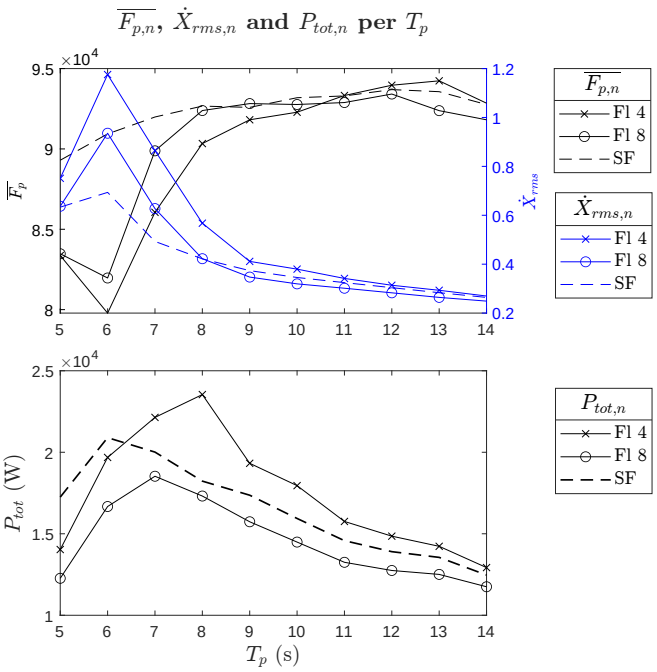

Fig. 8: Mean pumping force, RMS of the velocity and total power extracted by two floaters of the array compared to the single floater in all sea states with $H_s = 3m$

floater.

While the radiation of the single floater represents loss of potential power, in the array, this can lead to an increase of potential power at other, neighbouring elements. Fig. 7 depicts the root mean square (RMS) of the radiation force ($F_{r,\mathrm{RMS}}$) and the RMS of the excitation force ($F_{\mathrm{ex,RMS}}$), based on the time series of the sea state simulations for the entire range of T_p with fixed $H_s = 3m$, as the change in q factor from Fig. 3 is more significant at low H_s. The RMS values of the forces are shown for the single floater (SF), the mean of the entire array ($\overline{Array}$) and the minimum and maximum element of the array as an area around the mean.

Radiation effects are higher at short T_p, with a significant peak at $T_p = 6s$ for the array. The mean of $F_{r,\mathrm{RMS}}$ is larger than that of the single floater for the entire range of T_p and all elements of the array show higher radiation than the single floater at short T_p. The radiation effects at short T_p are also influencing the lower q factor in those sea states. Although the effect is larger in the array, the same behaviour can be noticed in the single floater which suggests it being connected to the single floater design and characteristics. Until $T_p = 11s$, the mean RMS excitation force of the array is higher than that of the single floater; this, in connection with the decrease in radiation force at $T_p = 8s$, leads to a q factor > 1. Furthermore, it is worth noting that the magnitude of the excitation force dominates the behaviour of the WECs.

4) Influence factors on Power Absorption: In Fig. 8, the mean pumping force, the RMS of the floaters' velocity and the total power of each sea state with $H_s = 3m$ are depicted. Two floaters of the array are selected to show the difference in power extraction and behaviour within the array. Floater 4 is placed in front of the central pillar and floater 8 is at the top rear of the array; these are selected because they show minimum and maximum radiation in Fig. 7, respectively. It can be observed that, with increasing radiation force, the displacement and velocity of the floaters show a peak ($T_p = 6s$), but the pumping force decreases, resulting in a lower power output. In this case, it is possible to see that the single floater shows the highest power extraction at slightly lower T_p compared to the floaters of the array. Differences within the array results worth noting are: at long T_p, the mean pumping force of floater 8 is higher than that of floater 4, but the total power is still lower than that of floater 4 which can be motivated by the velocity.

B. Influence of adaptability on interactions

The transmission ratio is adapted to maximise the power of the entire array and applied to all elements consistently; thus, the interactions between floaters are not significantly altered but mostly enhanced or reduced by the choice of transmission ratio.

1) Q Factor of Array: Before diving into more specific effects of α on the array's behaviour, an overview of the array's q factor is depicted in Fig. 9. With increasing level of adaptability the q factor of the array decreases and interaction effects are highlighted.

2) Q Factor of inidividual elements: Within the array with adaptability per sea state, the floaters with $q > 1$ and those with $q < 1$ show the same behaviour as in the case without adaptability ($\alpha = 1$). Considering the adaptability per time window, all floaters' q factor decreases and is smaller than 1 in most sea states and for most floaters. The local increase in performance at T_p = 7–8 and 10–11s is highlighted more than with

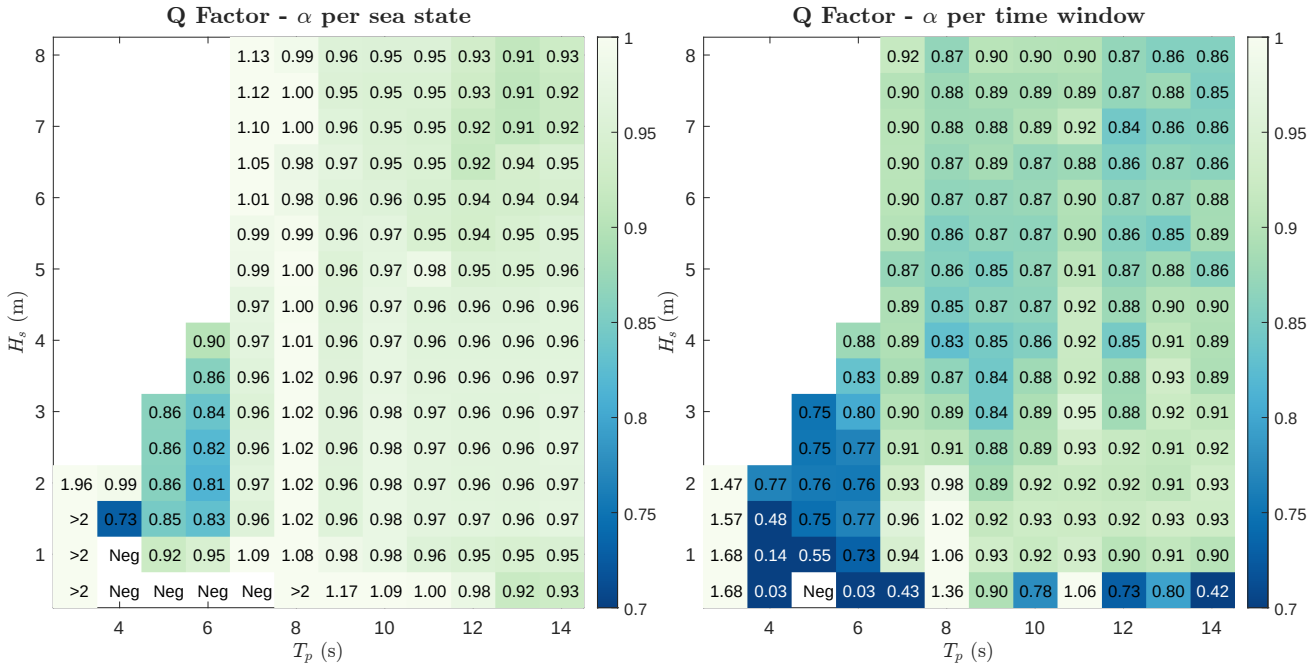

Fig. 9: Q factor of the WEC array for all sea states (a) with adaptability per sea state (b) with adaptability per time window

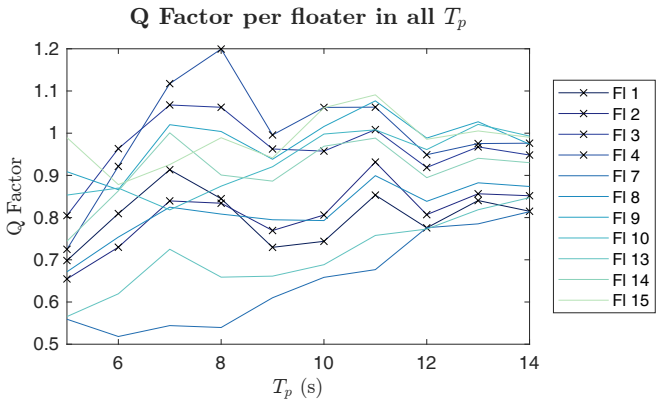

Fig. 10: The Q factors of all floaters of the array at sea state H_s 3m for all T_p show the different behaviour when applying the adaptability per time window.

lower adaptability levels and is mostly visible in the floaters around the central pillar, as reported in Fig.10.

3) Influence of transmission ratio on forces and velocity: When analysing the selection of α to maximise the total power per sea state, only slight changes to the selected α between single floater and array can be seen at long T_p (from 9s to 14s). At shorter T_p, the array selects smaller values for α compared to the single floater, especially at higher H_s. With the adaptability per time window, at low H_s the average α for the array is larger than for the single floater, while at higher H_s (from 3.5m) the average α is lower for the array. When the q factor shows lower values, the transmission ratio for the array is larger than that of the single floater, while with a larger q factor the transmission ratio is lower (for both levels of adaptability cases). This means that lighter PTO settings are chosen for the conditions in which the q factor is lower, leading to lower F_{pto} and higher displacement and velocity ($\dot{X}$).

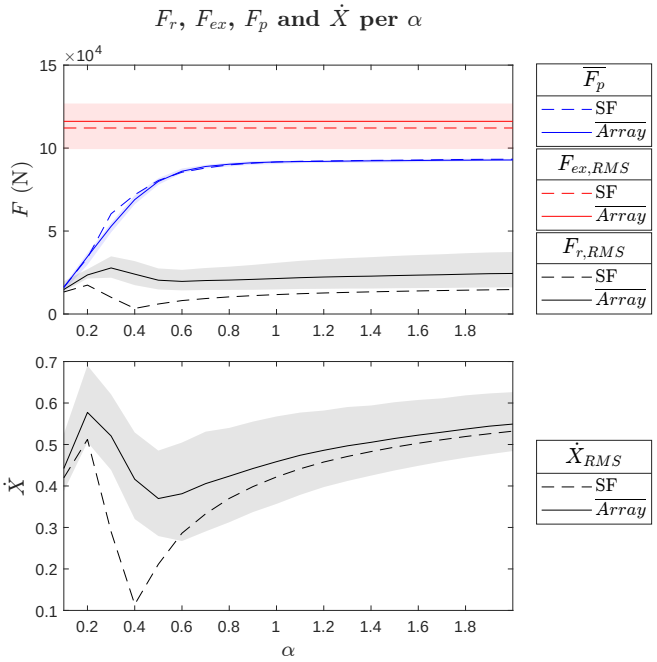

Fig. 11: Forces and velocity of single floater and WEC array for each α applied to the simulation of sea state $H_s = 3m$, $T_p = 8s$

The effect of a constant α for the simulation of a total sea state on the behaviour of the array and the single WEC is plotted in Fig. 11 for one sea state; these are the results from which the setting for the maximum power extraction with adaptability per sea state is chosen. The excitation force is not influenced by the transmission ratio, while the pumping force, radiation force and velocity show significant differences. It can be observed that the pumping force reaches its maximum value for both single floater and array due to the physical

constraints of the PTO system. The selected sea state for Fig. 11 shows high q factors in all adaptability cases and, to maximise the total power, the single floater applies $\alpha = 1.0$ and the array $\alpha = 0.9$ for the adaptability per sea state, in which the velocity and pumping force are at their optimum values. Although the velocity for the single floater and array are very high at low values of α, the pumping force is too low to reach the maximum power. The single floater shows a dip in F_r and velocity at the same value of α, while the array shows a peak of F_r at $\alpha = 0.3$ but a peak in velocity at $\alpha = 0.2$. The latter might be caused by subresonance due to effects of the Coulomb damping of the PTO system in addition to the hydrodynamic damping of the floaters [27]. From $\alpha = 0.6$ onward, the forces do not change significantly.

Further analysis of different sea states (as in Fig. 11) yields the following more general observations:

- At low H_s, the pumping force is larger than the excitation force at most α values
- With increasing T_p the difference between results of the single floater and the WEC array and the individual elements of the array decreases.
- The longer T_p is, the larger is the difference between F_{ex} and F_r, thereby decreasing the effect of radiation on the behaviour of the floaters.

4) Influence of adaptability on forces: With Fig. 12a and Fig. 12b it is possible to compare the resulting forces when different adaptability levels are applied. For the case with adaptability per sea state, α is selected to be slightly lower for the array at T_p 6–8s in which, as shown in Fig. 12a, the pumping force is lower and the the velocity is higher. A similar behaviour can be observed when applying adaptability per time window (Fig. 12b). The average α of adaptability per time window is higher than for adaptability per sea state within the sea states with $H_s = 3m$ considered in Fig. 12. Where dips in the pumping force are identified in the figures, the value of α is larger compared to the neighbouring sea states at short T_p (6s) and smaller at longer T_p (10–11s). The pumping force between the two adaptability cases shows significant differences; while the pumping force with adaptability per sea state remains approximately at its maximum, with adaptability per time window it decreases with increasing T_p. This is observed for both the single floater and the array. At higher T_p (e.g. $T_p = 11s$) the radiation force of the WEC array is higher, but the RMS of the velocity is slightly larger for the single floater.

5) Correlation between transmission ratio and excitation force: To understand more thoroughly how α is chosen per time window, the RMS mean excitation force for each time window and the selected α for one specific sea state are depicted in Fig. 13. The figure shows the occurrence of one specific combination between F_{ex} and α in a chosen sea state. From the analysis in previous sections, the excitation force has a higher influence on the performance of the floaters, thus, a relationship between this parameter and the selection of α can be extracted by fitting a nonlinear regression shown with the black line. In the figure, the RMS of the excitation force over all elements of the array is depicted. By analysing the excitation force of each element of the array separately and the selected α a trend can be identified: the floaters with higher q factor show a stronger correlation between the two variables.

C. Influence on power extraction of elements of the array

Analysing the q factor does not give the full picture on the power extraction performance of the WEC array. While the mean q factor decreases with increasing adaptability, the power extraction increases. Considering the incoming wave width of the array and that of 18 separate WECs shows that the array outperforms the single floater. It is also worth noting that with increasing adaptability the difference between the power extracted by the floaters performing best and worse in the array increases slightly; this might be enhanced due to α being constant over the entire array instead of selected individually per element of the array. When comparing what floaters performs best and worse, the floater with maximum power output varies more with increasing adaptability in the sea state matrix. Mainly floater 4 and, with higher adaptability, also floaters 10, 15, and 9 show maximum power extraction, while floater 7 shows lowest performance in most of the sea states independently from the adaptability level.

While assessing the adaptability per time window, it becomes clear that in different time windows different floaters in the array show maximum power extraction as depicted in Fig. 14. For sea state $H_s = 3.0m$ and $T_p = 8s$ the occurrence is relatively balanced and for sea state $H_s = 3.0m$ and $T_p = 13s$ floater 10 shows the maximum power in more than 30% of the time windows, although the floater that generates maximum power in the total simulation is actually floater 9.

V. Conclusion

The presented research focuses on the analysis of floater interactions in a dense WEC array with nonlinear PTO forces and a retroactively selected tuning parameter α. An MFT model iteratively combining time-domain and frequency-domain simulations is used to solve the equations of motion of the devices in irregular waves. The performance and behaviour of the elements of the array are compared to a single WEC in a range of sea states and depicted in matrix format. Overall, the results show that the excitation force magnitude is significantly larger than the radiation force in most sea states, thus making it the predominant force the devices are tuned for while, as the adaptability ratio α is applied consistently over the entire array, it does not alter the interaction effects but increases or decreases their effect. The transmission ratio α is selected to optimize the pumping force and velocity of the elements and a correlation between α and the excitation force of the elements can be identified. Furthermore, for all adaptability levels, the element of the array showing maximum power extraction depends on the peak period, T_p, of the sea state; the floater in front of the central pillar most frequently shows highest power extraction overall; and, the floaters at the front

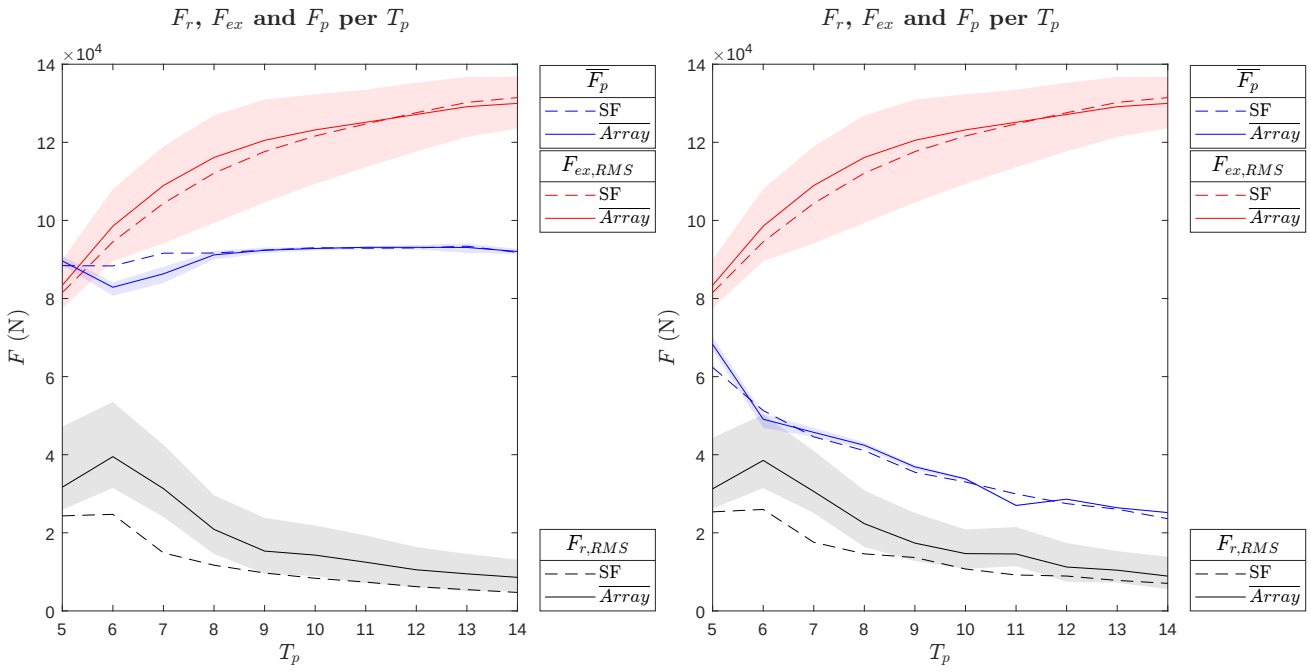

Fig. 12: Forces on single floater, mean array and minimum and maximum values of the array in all sea states with $H_s = 3m$; (a) with adaptability per sea state and (b) with adaptability per time window

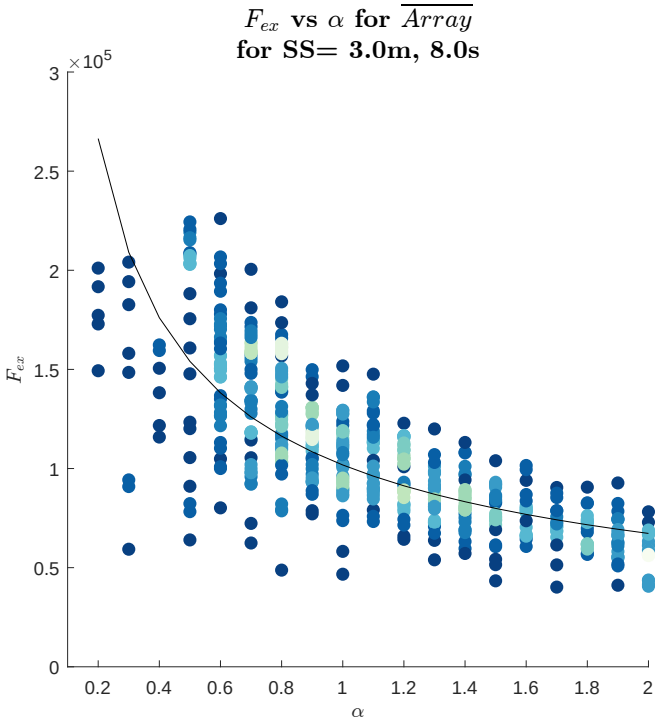

Fig. 13: Relationship between RMS of the mean excitation force of the array in each time window $\overline{F_{ex,RMS}}(tw)$ and the selected transmission ratio of each time window $\alpha(tw)$ of sea state $H_s = 3m$, $T_p = 8s$

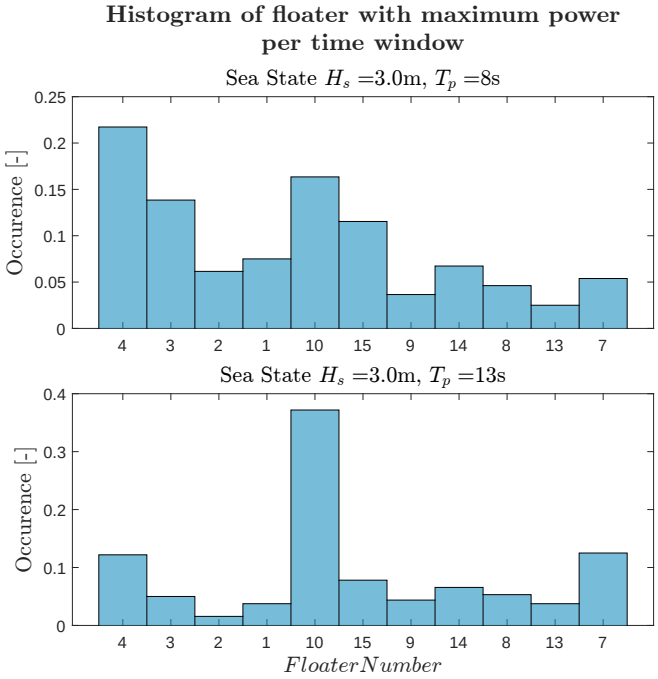

Fig. 14: Histogram of floater number that generates the maximum power in each time window of the simulation in two sea states

of the array in the direction of the incoming wave show higher power extraction.

Results specifically connected to the level of adaptability can be summarised as follows. With increasing adaptability:

- The power output of the single floater and WEC array increases but the q factor decreases.
- The difference in power output between the elements of the array increases overall.
- The transmission ratio α enhances the interaction effects, especially the positive effect of the central pillar.
- The difference in choice of α between single WEC and array increases.
- With adaptability per time window, in different sea states, the balance of power extraction per

element in the array is considerably different.

Future research will study interactions between floaters while applying adaptability within the simulation in order to include the motion of all elements with the selected transmission ratio and memory effect of their motion onto the next time window. Furthermore, adapting the PTO for each element separately could potentially influence the interactions within the array and should be studied in detail.

ACKNOWLEDGEMENT

The authors thank the Centre for Information Technology of the University of Groningen for their support and for providing access to the Peregrine high performance computing cluster.

REFERENCES

[1] C. E. Clark, A. Miller, and B. DuPont, "An analytical cost model for co-located floating wind-wave energy arrays," *Renewable Energy*, vol. 132, p. 885 – 897, 2019.

[2] X. Garnaud and C. C. Mei, "Wave-power extraction by a compact array of buoys," *Journal of Fluid Mechanics*, vol. 635, p. 389 – 413, 2009, all Open Access, Green Open Access.

[3] S. Michele and E. Renzi, "A second-order theory for an array of curved wave energy converters in open sea," *Journal of Fluids and Structures*, vol. 88, pp. 315–330, 2019.

[4] A. De Andrés, R. Guanche, L. Meneses, C. Vidal, and I. Losada, "Factors that influence array layout on wave energy farms," *Ocean Engineering*, vol. 82, p. 32 – 41, 2014.

[5] B. Yang, S. Wu, H. Zhang, B. Liu, H. Shu, J. Shan, Y. Ren, and W. Yao, "Wave energy converter array layout optimization: A critical and comprehensive overview," *Renewable and Sustainable Energy Reviews*, vol. 167, 2022.

[6] R. Ahamed, K. McKee, and I. Howard, "Advancements of wave energy converters based on power take off (pto) systems: A review," *Ocean Engineering*, vol. 204, p. 107248, 2020.

[7] B. Borgarino, A. Babarit, and P. Ferrant, "Impact of wave interactions effects on energy absorption in large arrays of wave energy converters," *Ocean Engineering*, vol. 41, pp. 79–88, 2012.

[8] D. Josh and C. Ronan, "Efficient nonlinear hydrodynamic models for wave energy converter design-a scoping study," *Journal of Marine Science and Engineering*, vol. 8, no. 1, 2020, all Open Access, Gold Open Access.

[9] A. Babarit, "On the park effect in arrays of oscillating wave energy converters," *Renewable Energy*, vol. 58, pp. 68–78, 2013.

[10] M. Folley and T. Whittaker, "Preliminary cross-validation of wave energy converter array interactions," in *Proceedings of the International Conference on Offshore Mechanics and Arctic Engineering - OMAE*, vol. 8, 2013, Conference paper.

[11] L. Wang, J. Isberg, and E. Tedeschi, "Review of control strategies for wave energy conversion systems and their validation: the wave-to-wire approach," *Renewable and Sustainable Energy Reviews*, vol. 81, p. 366 – 379, 2018.

[12] S. K. Poguluri, D. Kim, and Y. H. Bae, "Hydrodynamic analysis of a multibody wave energy converter in regular waves," *Processes*, vol. 9, no. 7, 2021, all Open Access, Gold Open Access.

[13] H. Gong, H. Shi, Z. Han, and F. Cao, "Experimental and numerical investigation on an optimization method of heaving buoy wave energy converter arrays based on a given target wave spectrum," *Ocean Engineering*, vol. 259, 2022.

[14] G. Bacelli, P. Balitsky, and J. V. Ringwood, "Coordinated control of arrays of wave energy devices-benefits over independent control," *IEEE Transactions on Sustainable Energy*, vol. 4, no. 4, p. 1091 – 1099, 2013, all Open Access, Green Open Access.

[15] M. Han, F. Cao, H. Shi, H. Kou, H. Gong, and C. Wang, "Parametrical study on an array of point absorber wave energy converters," *Ocean Engineering*, vol. 272, 2023.

[16] B. Guo and J. V. Ringwood, "A review of wave energy technology from a research and commercial perspective," *IET Renewable Power Generation*, vol. 15, no. 14, p. 3065 – 3090, 2021, all Open Access, Green Open Access.

[17] M. Göteman, M. Giassi, J. Engström, and J. Isberg, "Advances and challenges in wave energy park optimization—a review," *Frontiers in Energy Research*, vol. 8, 2020, all Open Access, Gold Open Access, Green Open Access.

[18] A. Trueworthy and B. Dupont, "The wave energy converter design process: Methods applied in industry and shortcomings of current practices," *Journal of Marine Science and Engineering*, vol. 8, no. 11, p. 1 – 49, 2020, all Open Access, Gold Open Access, Green Open Access.

[19] Y. Wei, J. Barradas-Berglind, Z. Yu, M. van Rooij, W. Prins, B. Jayawardhana, and A. Vakis, "Frequency-domain hydrodynamic modelling of dense and sparse arrays of wave energy converters," *Renewable Energy*, vol. 135, p. 775 – 788, 2019, all Open Access, Green Open Access.

[20] Y. Wei, A. Bechlenberg, B. Jayawardhana, and A. Vakis, "Modelling of a wave energy converter array with non-linear power take-off using a mixed time-domain/frequency-domain method," *IET Renewable Power Generation*, vol. 15, no. 14, p. 3220 – 3231, 2021, all Open Access, Gold Open Access, Green Open Access.

[21] J. van Til, F. Alijani, S. Voormeeren, and W. Lacarbonara, "Frequency domain modeling of nonlinear end stop behavior in tuned mass damper systems under single- and multi-harmonic excitations," *Journal of Sound and Vibration*, vol. 438, pp. 139–152, 2019.

[22] A. Mérigaud and J. V. Ringwood, "A nonlinear frequency-domain approach for numerical simulation of wave energy converters," *IEEE Transactions on Sustainable Energy*, vol. 9, no. 1, pp. 86–94, 2018.

[23] W. Chen, F. Gao, X. Meng, and J. Fu, "Design of the wave energy converter array to achieve constructive effects," *Ocean Engineering*, vol. 124, pp. 13–20, 2016.

[24] B. Howey, K. M. Collins, M. Hann, G. Iglesias, R. P. Gomes, J. C. Henriques, L. M. Gato, and D. Greaves, "Compact floating wave energy converter arrays: Inter-device mooring connectivity and performance," *Applied Ocean Research*, vol. 115, 2021, all Open Access, Green Open Access, Hybrid Gold Open Access.

[25] A. Bechlenberg, Y. Wei, B. Jayawardhana, and A. I. Vakis, "Analysing the influence of power take-off adaptability on the power extraction of dense wave energy converter arrays," *Renewable Energy*, vol. 211, pp. 1–12, 2023.

[26] C. Beels, J. Henriques, J. De Rouck, M. Pontes, G. De Backer, and H. Verhaeghe, "Wave energy resource in the north sea," in *EWTEC 2007-7th European Wave and Tidal Energy Conference*, 2007.

[27] L. Marino and A. Cicirello, "Coulomb friction effect on the forced vibration of damped mass-spring systems," *Journal of Sound and Vibration*, vol. 535, 2022, all Open Access, Green Open Access, Hybrid Gold Open Access.